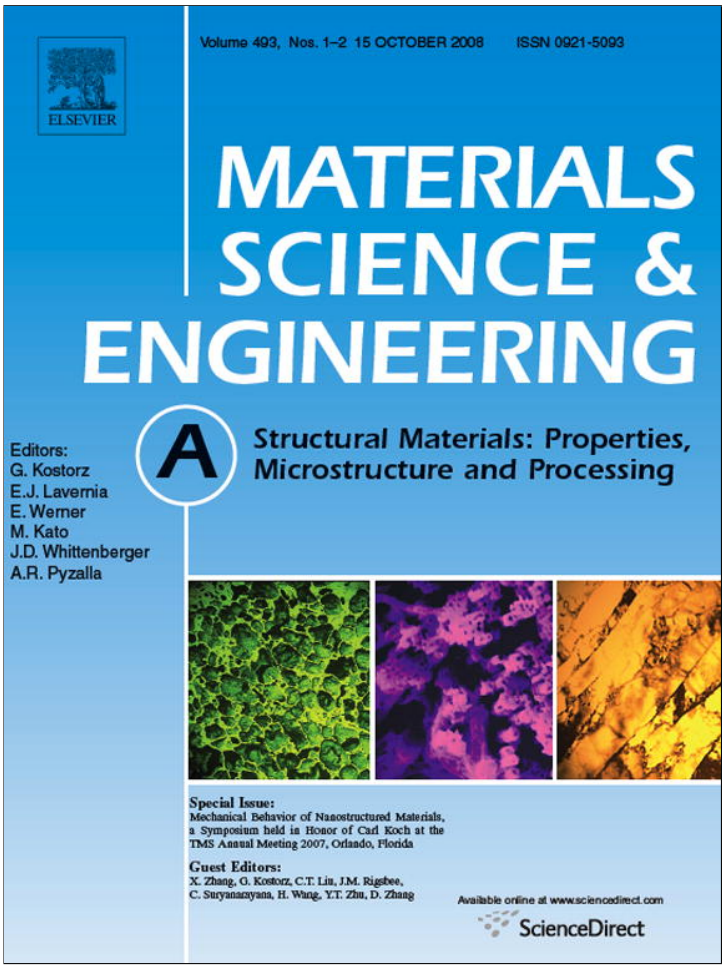

ELSEVIER

Materials Science and Engineering A 493 (2008) 65–70

MATERIALS SCIENCE & ENGINEERING A

www.elsevier.com/locate/msea

Grain size dependent shear instabilities in body-centered and face-centered cubic materials

Shailendra P. Joshi *, K.T. Ramesh

Room 223, Latrobe Hall, Department of Mechanical Engineering, The Johns Hopkins University, 3400 North Charles Street, Baltimore, MD 21218, USA

Received 19 February 2007; received in revised form 15 June 2007; accepted 20 June 2007

Abstract

The grain size dependence of the mechanical response has been a topic of immense interest in nanostructured (NS) materials. Most NS metals produced by grain refinement processes show characteristically different work hardening and rate sensitivity from their coarse-grained counterparts. These differences, coupled with novel deformation mechanisms in NS materials, have direct implications on the stability of the plastic deformation process. Recently, we proposed a model for grain rotation based geometric softening within a visco-plastic constitutive setting to investigate grain size dependent shear instabilities in NS metals. Using this model, we investigate the effects of internal material hardening on the shear instabilities in NS body-centered cubic and face-centered cubic metals at quasi-static loading rates. At small grain sizes, the model predicts occurrence of the shear bands for both b.c.c. and f.c.c. materials as a consequence of the dominance of geometric softening over material hardening. However, in NS face-centered cubic materials the occurrence of instability is delayed due to elevated rate sensitivity compared NS body-centered cubic materials.

Keywords: Nanostructured b.c.c. and f.c.c. metals; Shear instability; Grain rotation; Strain hardening and strain rate sensitivity

1. Introduction

Grain refinement in metals gives rise to microscopic deformation mechanisms that are not commonly observed in their coarse-grained counterparts [1–5]. Several researchers have provided mechanistic descriptions of the deformation mechanisms that may occur within the grains and at the grain boundaries (gb) as a function of grain size [6,7]. On a macroscopic scale, many nanostructured (NS) materials exhibit lack of strain hardening beyond small strains. Further, in pure body-centered cubic (b.c.c.) structures the strain rate sensitivity decreases as the grain size decreases, whereas the reverse is true for face-centered cubic (f.c.c.) structures [8]. Quasi-static compression on NS Fe [9–11] indicated inhomogeneous plastic flow through shear banding; at larger grain sizes the material exhibited homogeneous plastic flow [10]. Through transmission electron microscopy (TEM) of NS Fe, Wei et al. [11] showed that the grains experienced rotation and alignment during deformation to form bands with textures that allow easy slip in certain orientations. Further, they also observed uniform microstructures and the absence of recrystallization in the bands. Based on these characteristics, the authors postulated a geometric softening mechanism involving grain rotation that results in the localization of plastic flow in narrow regions called shear bands (Fig. 1, provided by Prof. Q. Wei). These shear bands were oriented approximately 45° to the compression axis and their thickness was about 50 times the grain size [10]. Experiments on NS Cu [12] also showed shear failure instead of necking under quasi-static uniaxial tension, which they attributed to reduced strain hardening compared to the coarse-grained (CG) Cu. Shear bands have been reported in equal-channel angular pressed (ECAP) Al with 590 nm grain size subjected to quasi-static uniaxial compression [13], although shear bands are not commonly observed in NS f.c.c. metals under compression.

In nanocrystalline materials, shear bands severely limit the ductility, and it is therefore important to understand the underlying mechanisms for their occurrence.

Although several researchers have investigated shear banding in single crystals and CG polycrystals under different states of loading [14–17], very few grain size dependent shear-band models have been presented. While strain gradient theories [18,19] incorporate length scales in to the model allowing prediction

* Corresponding author. Tel.: +1 410 516 5162; fax: +1 410 516 7254.
E-mail address: spjoshi@jhu.edu (S.P. Joshi).

0921-5093/$ – see front matter © 2007 Elsevier B.V. All rights reserved.
doi:10.1016/j.msea.2007.06.094

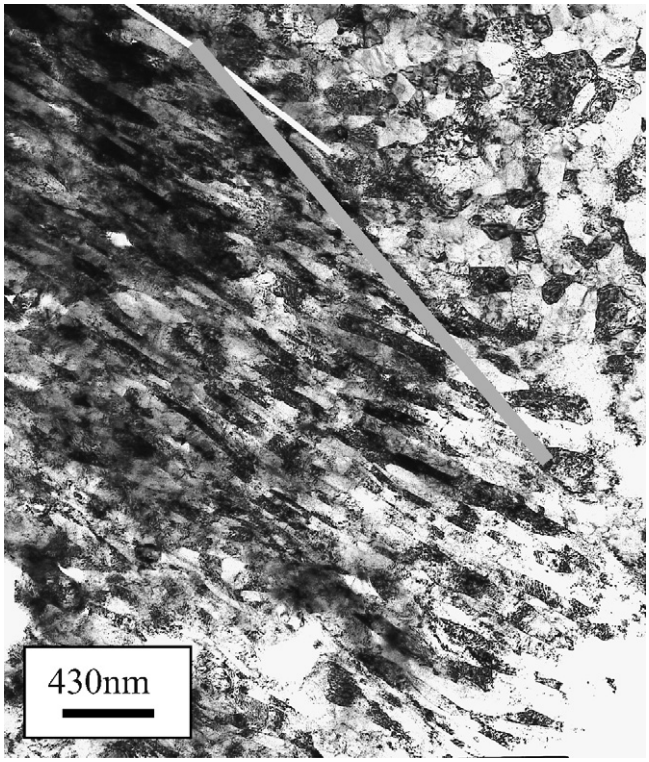

Fig. 1. TEM image indicating shear band in Fe of 110 nm grain size. The solid line (magenta) indicates the sharp transition region of the band. Note the highly oriented grain structure inside the band and equiaxed, random structure outside the band (courtesy Q. Wei).

of shear-band thicknesses without mesh dependency, they do not explicitly account for the grain size effect. Crystal plasticity models [20,21] augmented with constitutive descriptions for the gb phase have been presented to predict trends for the grain size dependent response in polycrystalline materials but these are very intensive computations that must prescribe the properties of a gb phase. Recently, we have developed a model that considers the development of shearing instabilities resulting from grain rotation driven geometric softening [22]. The grain size enters naturally through the grain rotation mechanism.

Grain size along with the crystal structures plays a governing role in determining the strain rate sensitivity [8,23], which is an important mechanism for stabilizing the deformation process. In this article, we use the recently developed model [22] to investigate the effect of crystal structure on the grain rotation driven shear instabilities in nanostructured metals. We focus on the b.c.c. (Fe) and f.c.c. (Cu) structures and their role in the development of shear bands. In the next section, the shear-band model is presented briefly and the results are discussed in the subsequent sections.

2. Governing equations

Consider an infinitely long slab with finite thickness (Fig. 2), W (in the X direction) subjected to a constant nominal quasi-static shear strain rate ($\dot{\gamma}_a$). Ignoring the inertial effects at these quasi-static loading rates and assuming isothermal conditions,

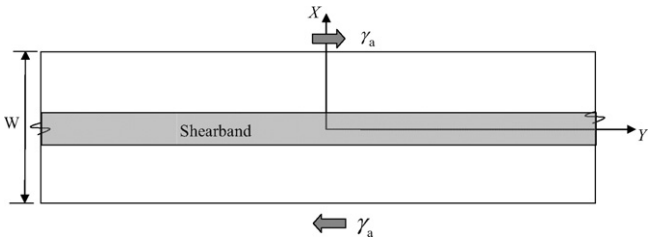

Fig. 2. Schematic of the shear-band problem.

the governing equations for a one-dimensional shear problem are

$$\frac{\partial \tau}{\partial X} = 0 \tag{1}$$

The material is assumed to be elastic/visco-plastic, so that

$$\dot{\tau} = \frac{\partial \tau}{\partial t} = \mu \bar{\dot{\gamma}}_e = \mu(\dot{\gamma}_a - \bar{\dot{\gamma}}_p) \tag{2}$$

where μ is the elastic shear modulus, $\bar{\dot{\gamma}}_e$ the average elastic strain rate, and $\bar{\dot{\gamma}}_p$ is the average plastic strain rate $\left(= 1/W \int_0^W \dot{\gamma}_p \, dX\right)$, and the total applied strain rate is $\dot{\gamma}_a = \bar{\dot{\gamma}}_e + \bar{\dot{\gamma}}_p$. Since it is known that the rate sensitivity varies with grain size and the crystal structure [8], a visco-plastic constitutive law is assumed for the evolution of plastic strain

$$\dot{\gamma}_p = \dot{\gamma}_0 \left\langle \left\{ \frac{\tau}{\tau_0} \frac{1}{(1 - \bar{c}\phi)} \left(1 + \frac{\gamma_p}{\gamma_0}\right)^{-n} \right\}^{1/m} - 1 \right\rangle \tag{3}$$

where $\langle \cdot \rangle$ is defined as $\langle f \rangle = (f + |f|)/2$, ϕ an internal variable (described below) and γ_p is the plastic strain. The terms $\dot{\gamma}_0$ τ_0, γ_0, n and m in Eq. (3) represent the characteristic strain rate, yield strength (of the polycrystalline material), yield strain (corresponding to τ_0), strain hardening index, and strain rate sensitivity, respectively. Note, both n and m depend on the grain size and the crystal structure (f.c.c. versus b.c.c.) [8]. The form of Eq. (3) resembles that of the typical constitutive laws employed to material behavior over a range of strain rates and includes a thermal softening term [24]. We retain the simple physical description of the material behavior in terms of its material hardening and replace the thermal softening term by an equivalent geometric softening term. The term $(1 - \bar{c}\phi)$ represents the softening response in that $\bar{c}$ $\left(= 1 - \frac{\tau_{s0}}{\tau_{h0}}\right)$ is the ratio of the single crystal yield strengths in the softest (τ_{s0}) and hardest (τ_{h0}) orientations, respectively (Fig. 3a). The internal variable ϕ is defined as the number fraction of grains in a given region that have the soft orientation aligned to the shearing direction: $\phi(t) = \frac{N_s}{N_b}$, where N_s is the number of grains in a representative volume element (RVE) (total number of grains, N_b) that have the soft orientation aligned with the shearing direction (Fig. 3b). With incremental loading a crystal rotates to align its soft orientation along the shearing direction and ϕ represents the homogenized description of this rotation over an RVE.

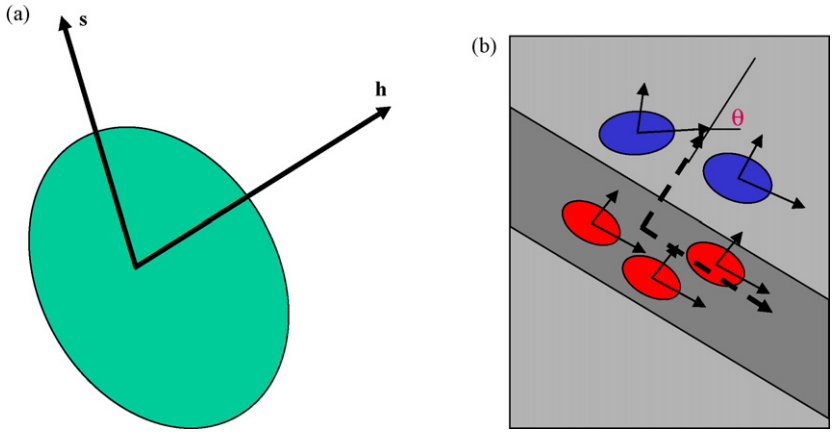

Fig. 3. (a) Schematic of a single crystal showing hardest (h) and softest (s) orientations with respect to the shear yield stress. (b) Schematic of the definition of grain orientation θ. The internal variable ϕ is the weighted average of the grain orientation in a region; $\phi = 1$ in the shear band.

The evolution of ϕ is then the representation of the evolution of rotation of the grains

$$\dot{\phi} = \psi\dot{\gamma}_{\mathrm{p}} + D_{\mathrm{r}}\frac{\partial^2\phi}{\partial X^2} \tag{4}$$

A detailed derivation of Eq. (4) is given in Ref. [22]. The first component in Eq. (4) represents the contribution of overall plasticity to grain rotation, i.e., it represents rotation of an ensemble of grains (E) embedded in a viscoplastic region (V) (Fig. 4a). The term ψ indicates the ease with which a grain can rotate rigidly in the surrounding viscoplastic sea and is of the order 10 for NS materials. The second component arises from the contribution of inter-granular interaction within the grain ensemble (E) (Fig. 4b). This region is defined by a length-scale L defining the region that is influenced by the rotation of the central grain. It is the region surrounding the rotating grain that "feels" the rotation and accomodates it through combined rotation and plastic slip in the neighbouring grains; thus, it is a plastically dissipative length-scale accomodating grain rotation. The coefficient D_{r} describes this domain of influence (of radius L, Fig. 4b) of the grain rotation through inter-granular interaction derived from elasto-plastic contact mechanics [22] at the grain level and homogenized over the RVE:

$$D_{\mathrm{r}} = \frac{1}{j\eta}\left(\frac{\mu d^2}{2-\nu}\right) \tag{5}$$

In Eq. (5), μ is the elastic shear modulus, d the grain size, υ the Poisson's ratio, $j(=L/d)$ the number of grains over length L influenced by grain rotation and $\eta(=\tau_{\mathrm{s0}}/\dot{\gamma}_0)$ is the viscosity representing the resistance of the surrounding grains.

3. Numerical simulations

We consider an infinitely long slab of width (W) equal to 300 μm subjected to a quasi-static nominal shear-strain rate $\dot{\gamma}_{\mathrm{a}} = 5 \times 10^{-4}\,\mathrm{s}^{-1}$. To illustrate the model, we consider the case of NS Fe (Table 1). We assume an initial defect distribution ϕ_i in the form of a Gaussian function

$$\phi_i(X) = \phi_0\,\exp\left[-\kappa\left(\frac{X}{W} - 0.5\right)^2\right] \tag{6}$$

where ϕ_0 (=0.005) is the maximum value of ϕ, κ (=50,000) is a dimensionless parameter that controls the base width of the function. We assume far-field value of $\phi = 0$, indicating that on an average the grain orientations are random sufficiently away

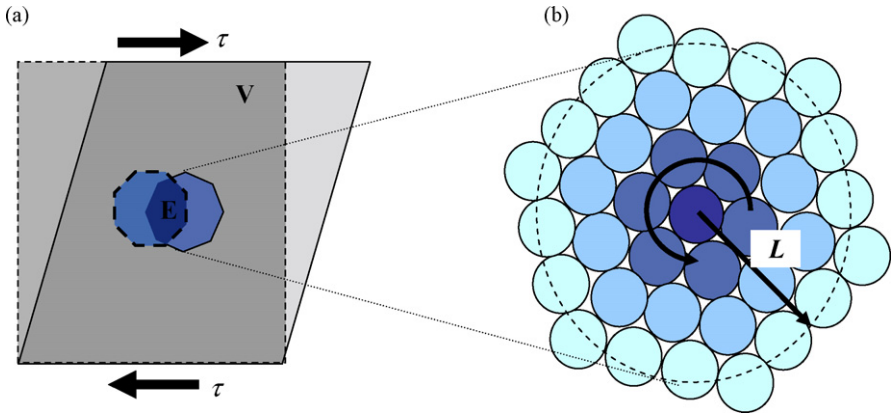

Fig. 4. (a) Schematic illustrating the rotation of region (E) comprising ensemble of rigid grains embedded in a visco-plastic medium (V) subjected to shear and (b) Enlarged view of the rotation mechanism in the region (E) due to grain rotation mediated inter-granular interaction.

Table 1
Material parameters for polycrystalline Fe used in the simulations

Parameter	Value
d (nm)	300
μ	76
ν	0.3
$\dot{\gamma}_0$ (s^{-1})	5×10^{-4}
τ_0 (MPa)	900
n	0.01
m	0.005
$\bar{c}$	0.07
ψ	10

from the perturbed region. The initial conditions are: $\tau(X,0) = 0$, $\phi(X,0) = \phi_i(X)$, $\gamma(X,0) = 0$, $\dot{\gamma}(X, 0) = \dot{\gamma}_a$. Eqs. (1)–(4) are solved numerically using the Euler forward difference scheme. The slab is discretized into 20,000 segments with 20,001 nodes ($\Delta X = 15$ nm). The parameter $\bar{c}$ is obtained from the results of [25] on iron single crystals, as the ratio of the flow strengths corresponding to the strongest and softest orientations at large strains that are typically experienced during severe plastic deformation.

The overall stress–strain response (Fig. 5) for a defect-free material is presented (curve A) and compared with the response obtained from a sample with the perturbation (curve B). For a material with an initial distribution in ϕ (Eq. (6)), the sample exhibits a brief period of strain hardening following yield. The strain hardening is followed by a rapid drop in the stress corresponding to severe localization, with the magnitude of the drop determined by the material hardening and the anisotropy parameters. Following the stress drop, a softening response is observed. Such a macroscopic softening response of a strain hardening material indicates the dominance of geometric softening over material hardening [5].

With increasing strain, the grain reorientation saturates ($\phi = 1$) in the localized region. Defining the thickness of a fully developed shear band as a region where ϕ reaches the maximum value the development of the thickness of the shear band is shown (Fig. 5) as a function of overall strain. The shear-band broadening with strain is a consequence of the material hardening together with rotational diffusion (Eq. (4)).

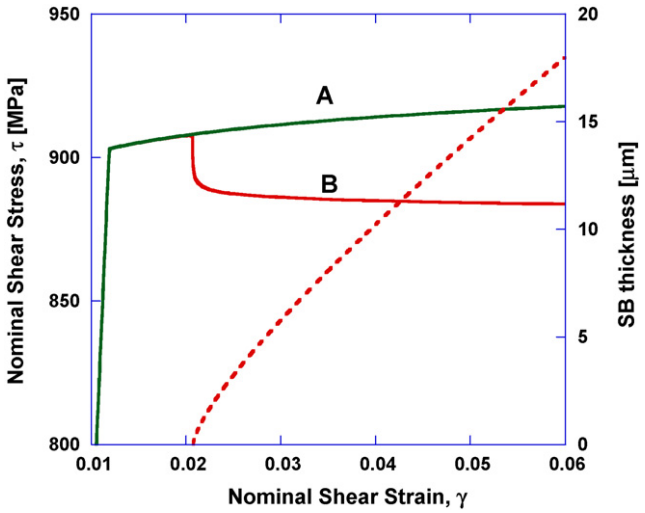

Fig. 5. Overall shear stress–shear strain response for a defect-free ultrafine Fe (curve A) and with an initial defect in ϕ (curve B) subjected to $\dot{\gamma}_a$ of 5×10^{-4} s^{-1}. The dashed curve indicates the development of the shear-band thickness corresponding to curve B.

3.1. Effect of strain hardening

Strain hardening (n) and strain rate sensitivity (m) tend to stabilize the deformation process with high values of n and m resulting in extended regimes of homogeneous deformation. Geometric softening triggered by grain reorientation (ϕ) acts as a destabilizing mechanism that competes with the material hardening. Our results in Ref. [22] show that the presence of strain hardening delays the onset of instability, and at high values of n the material does not show localization even at large strains (>30%). If localization does occur, the band broadens much more rapidly in the presence of strain hardening in comparison to the elastic-perfectly plastic material.

3.2. Effect of strain rate sensitivity: comparison of Fe and Cu responses

While, many NS metals (especially those produced by grain refinement process) exhibit diminished strain hardening, the rate sensitivity depends on the crystal structure. Most b.c.c. materials exhibit reduced rate sensitivity in the ultrafine (UFG) or NS regimes compared with the CG regime whereas the reverse is true for the f.c.c. materials. For the purpose of comparison, we consider b.c.c. Fe and f.c.c. Cu, with the following parameters: 80 nm b.c.c. Fe with $\sigma_y = 2500$ ($\tau_0 = \sigma_y/\sqrt{3} = 1440$ MPa), $n = 0.01$ and $m = 0.005$ [10], and 60 nm f.c.c. Cu ($\mu = 46$ GPa) with $\sigma_y = 600$ MPa ($\tau_0 = 381$ MPa), $n = 0.01$ and $m = 0.03$ [12]. To illustrate the grain size effect, we compare these with their corresponding responses for a larger grain size (~1 μm).

Note that the processing routes normally involve severe plastic deformations and therefore, we require the crystal strengths at large strains. The factor $\bar{c}$ is chosen to be 0.15 for f.c.c. Cu (based on the data given in Refs. [26,27]). This ratio is very large as compared to the ratio for Fe (Table 1). It is difficult in general, to make direct quantitative comparisons with the experiments due to uncertainties in these material parameters for real NS materials, but we provide a qualitative comparison with the experiments here. The length scale (Fig. 3b) is assumed to be constant for all the cases ($L = 1$ μm), which in conjunction with the material hardening parameters determines the broadening rate of the band.

Fig. 6 shows the shear stress–shear strain responses for a constant applied shear strain rate of 1×10^{-3} s^{-1}. The results are shown for two different grain sizes for both the Fe and the Cu. As expected, the NS Fe shows localization due to the lack of material hardening. However, in the case of 1 μm Fe (with $\tau_0 = 290$ MPa, $n = 0.07$, $m = 0.015$, [22]) the plastic flow is of strain-hardening type and does not exhibit localization. Similar experimental observations were made by Jia et al. [10]. In comparison, NS Cu, which is f.c.c., also exhibits strain hardening up to a strain of about 0.031 followed by a very small drop in

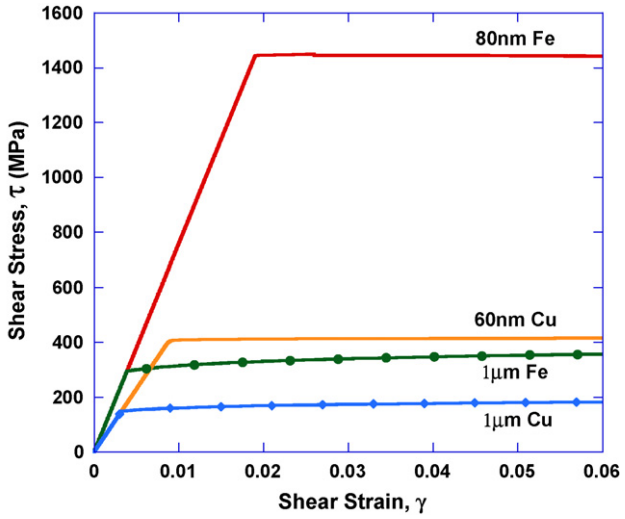

Fig. 6. Shear stress–shear strain responses for Fe and Cu subjected to $\dot{\gamma}_a = 1 \times 10^{-3}\ s^{-1}$.

the stress (not perceptible in Fig. 6). As discussed in Ref. [22], the higher the plastic anisotropy ($\bar{c}$) the more rapid the localization. For NS Cu, the high $\bar{c}$ is counter balanced by the high rate sensitivity. Although this is not visible in Fig. 6, the softening term $(1 - \bar{c}\phi)$ in the constitutive law (Eq. (3)) wins the competition due to high $\bar{c}$. However, the resulting localization and the corresponding softening are not persistent as the local material hardening (due to high m) is restored immediately thus impeding a runaway instability. This "diffuse" localization result is qualitatively consistent with the observations by Cheng et al. [12] for NS Cu. As in the case of Fe, the 1 μm grain-sized Cu (with $\tau_0 = 145$ MPa [7], $n = 0.1$ [28], and $m = 0.01$ [8]) also does not show localization.

Fig. 7 shows the development of the band with respect to average plastic shear strain. Despite the lack of strain hardening, the influence of the rate sensitivity is significant as the shear band occurs much later in NS Cu than in NS Fe. The delayed localization is remarkable considering the high strength anisotropy of

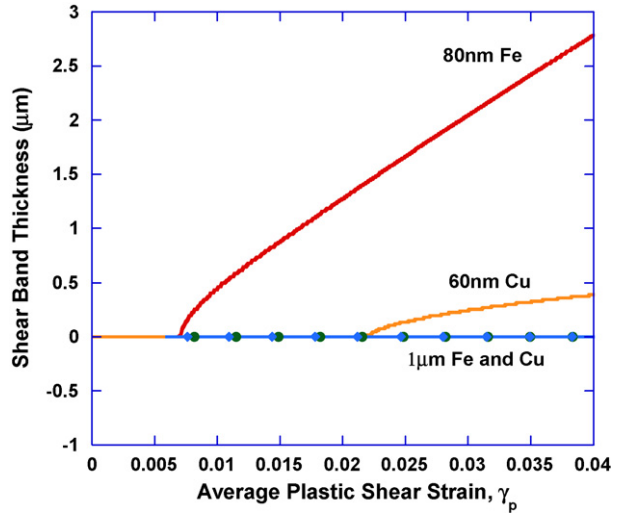

Fig. 7. Evolution of shear-band thickness for the cases of Fe and Cu.

NS Cu in comparison to NS Fe. For the same strain hardening, the broadening rate of the band (determined by D_r in Eq. (5)) for NS Cu is slower than that of NS Fe because Cu is elastically and plastically softer than Fe (note that D_r is also affected by the smaller grain size). Further, the local hardening makes the band in Cu very diffuse (described by the slope of the perturbation). For NS Fe the computed shearband thickness is about 2 μm at 2% plastic shear strain, which is comparable to the thicknesses observed by Wei (Fig. 1) for 110 nm grain size. Note that for a given material the higher the rate sensitivity the faster is the broadening of the band which relates to a more diffused transition region of the band (a similar observation was made in [12], indicating diffuse bands for materials with higher m).

Thus, in the presence of plastic anisotropy shear instabilities are inevitable in low strain hardening NS materials, but could be delayed due to high rate sensitivities. It is apparent that the quantitative estimates of shear-band onset and growth require much more detailed information on the crystallographic response at large strains.

4. Closing remarks

A recently developed shear-band model based on grain reorientation has been applied to NS f.c.c. and b.c.c. metals subjected to quasi-static rates of loading. Analogous to the experimental observations, the model predicts inhomogeneous plastic flow through shear banding at small grain sizes in b.c.c. materials as a result of the dominance of grain rotation driven geometric softening over material hardening whereas at larger grain sizes shear bands are not seen. In NS f.c.c. materials, the elevated rate sensitivity delays the occurrence of instability and may impede runaway localization. The model also predicts shear-band broadening that depends on the crystal structure and the grain size.

Acknowledgements

The authors would like to thank Prof. Q. Wei (UNC, Charlotte) for providing the TEM image in Fig. 6. This work was performed under the auspices of the Center for Advanced Metallic and Ceramic Systems (CAMCS) at the Johns Hopkins University, supported by the Army Research Laboratory under the ARMAC-RTP Cooperative Agreement nos. DAAD19-01-2-0003 and W911NF-06-2-0006.

References

[1] J.W. Cahn, J.E. Taylor, Acta Mater. 52 (2004) 4887–4898.
[2] M.Y. Gutkin, I.A. Ovid'ko, Appl. Phys. Lett. 87 (2005) 1–3 (article 251916).
[3] A.J. Haslam, D. Moldovan, V. Yamakov, D. Wolf, S.R. Phillipot, H. Gleiter, Acta Mater. 51 (2003) 2077–2112.
[4] M. Murayama, J.M. Howe, H. Hidaka, S. Takaki, Science 295 (2002) 2433–2435.
[5] W. Yang, H. Wang, J. Mech. Phys. Solids 52 (2004) 875–889.
[6] K.S. Kumar, H. Van Swygenhoven, S. Suresh, Acta Mater. 51 (2003) 5743–5774.
[7] M.A. Meyers, A. Mishra, D.J. Benson, Prog. Mater. Sci. 51 (2006) 427–556.

[8] Q. Wei, S. Cheng, K.T. Ramesh, E. Ma, Mater. Sci. Eng. A 381 (2004) 71–79.
[9] J.E. Carsley, A. Fisher, W.W. Milligan, E.C. Aifantis, Metall. Mater. Trans. A 29 (1998) 2261–2271.
[10] D. Jia, K.T. Ramesh, E. Ma, Acta Mater. 51 (2003) 3495–3509.
[11] Q. Wei, D. Jia, K.T. Ramesh, Appl. Phys. Lett. 81 (2002) 1240–1242.
[12] S. Cheng, E. Ma, Y.M. Wang, L.J. Kecskes, K.M. Youssef, C.C. Koch, U.P. Trociewitz, K. Han, Acta Mater. 53 (2005) 1521–1533.
[13] C.Y. Yu, P.L. Sun, P.W. Kao, C.P. Chang, Scripta Mater. 52 (2005) 259–263.
[14] R.J. Asaro, A. Needleman, Acta Mater. 33 (1985) 923–953.
[15] I.L. Dillamore, Met. Sci. 13 (1979) 73–77.
[16] S.V. Harren, H.E. Deve, R.J. Asaro, Acta Metall. 36 (1988) 2435–2480.
[17] S. Yang, B. Bacroix, Int. J. Plast. 12 (1996) 1257–1285.
[18] J.E. Carsley, W.W. Milligan, Z.X.H.E.C. Aifantis, Scripta Mater. 36 (1997) 727–732.
[19] X.H. Zhu, J.E. Carsley, W.W. Milligan, E.C. Aifantis, Scripta Mater. 36 (1997) 721–726.
[20] H. Fu, D.J. Bensom, M.A. Meyers, Acta Mater. 52 (2004) 4413–4425.
[21] M. Kuroda, V. Tvergaard, J. Mech. Phys. Solids 54 (2006) 1789–1810.
[22] S.P. Joshi, K.T. Ramesh, Acta Mater. 56 (2008) 282–291.
[23] R.J. Asaro, S. Suresh, Acta Mater. 53 (2005) 3369–3382.
[24] Q. Wei, T. Jiao, K.T. Ramesh, E. Ma, L.J. Kecskes, L. Magness, R. Dowding, V.U. Kazykhanov, R.Z. Valiev, Acta Mater. 54 (2006) 77–87.
[25] W.A. Spitzig, A.S. Keh, Acta Metall. 18 (1970) 611–622.
[26] X. Huang, A. Borrego, W. Pantleon, Mater. Sci. Eng. A 319–321 (2001) 237–241.
[27] U.F. Kocks, H. Mecking, Prog. Mater. Sci. 48 (2003) 171–273.
[28] X. Huang, N. Hansen, Mater. Sci. Eng. A 387–389 (2004) 186–190.